Analytical and Experimental Investigation of Substrate Permittivity and Loss up to 67 GHz

Patrick Seiler[*1], **Bernhard Klein**[*2], and **Dirk Plettemeier**[*3], Non-members

ABSTRACT

In this paper, we characterize the substrate permittivity and overall loss of different planar transmission lines (TLs) such as microstrip (MS), coplanar waveguide (CPW) and grounded CPW (GCPW) using on-wafer probes and a thru-reflect-line (TRL) calibration technique. The theory for calculation of the related effective permittivity from S-Parameter measurements is given and numerical simulations are being used for a fast and precise mapping of the effective permittivity $\varepsilon_{r,eff}$ to the physical value ε_r of the TL's substrate. The method presented can be used for higher frequencies, as long as single mode operation of the TLs is ensured. Thus, an overview on higher order modes in TLs and design rules to suppress them is given. The results up to 67 GHz for the aforementioned TL on a conventional RF substrate are presented and used to evaluate approximate models known from publications.

Keywords: Permittivity measurement, dielectric properties, planar transmission lines, TRL, higher order modes.

1. INTRODUCTION

The knowledge of material properties such as the frequency-dependent permittivity ε_r (sometimes still referred to as dielectric constant) is crucial to allow for a proper design procedure of most electronic applications. Since the libraries of common design tools as well as most material vendors only give frequency-limited or even static data on the dielectric properties of materials, the simulation accuracy of electromagnetic problems is decreased as material dispersion becomes more significant with increasing frequency. Thus, the interest in supplying developers and design tools with sufficient material data especially for higher frequencies remains still unchanged and drives the development of appropriate material characterization techniques.

Over the last decades, transmission/reflection methods for dielectric material characterization have been investigated thoroughly. Applying these methods, a sample material filling the cross-section of a rectangular waveguide or coaxial transmission line cell could be easily characterized over the working frequency range of the cell [1], [2].

Focusing on planar technology, these methods can be adapted to planar transmission lines under certain conditions [2] and enable a calculation of the effective permittivity $\varepsilon_{r,eff}$ of the TL's substrate from S-Parameter measurements. Subsequently, an evaluation of the dispersion effects allows for a mapping of $\varepsilon_{r,eff}$ to ε_r, which represents the actual, physical value of the substrate's permittivity.

For the most relevant TLs with respect to applications such as MS, CPW and GCPW, dispersion models exist, which perform the subsequent permittivity mapping in a quasi-analytic way. These models often rely on sophisticated curve fits (such as [3] for MS, [4] for GCPW or [5] for CPW) or are mere quasi-static approximations [6], which do not consider dispersion effects at all. Especially if frequency and thus dispersion is increasing, these models can only provide limited accuracy. To avoid the issues using these techniques and be able to properly account for the dispersion even for higher frequencies, we will use Finite Element Method (FEM) simulations to evaluate the dispersion and perform a fast and easily implemented mapping of the permittivity.

The following section 2 gives a general derivation of the permittivity from the Maxwell equations. This general approach is followed by the necessary relations to extract the propagation constant as well as the respective effective permittivity and loss from S-Parameter measurements of TLs. In section 3, higher order modes in planar transmission lines and design rules to suppress them as well as TL radiation are briefly outlined. In section 4, related measurements on a wafer prober using MS, CPW and GCPW will be shown. The extracted values for the effective permittivity of the respective TLs substrate will then be mapped to the physical value and compared to the value given by approximate models known from publications. In addition, the determined overall loss of the measured TL will be given and observed deviations will be discussed.

Manuscript received on February 17, 2015 ; revised on March 24, 2015.

* The authors are with the Communications Lab and Chair for RF Engineering at the Cluster of Excellence 'Center for Advancing Electronics Dresden', Technische Universität Dresden, Germany, E-mail: patrick.seiler@tu-dresden.de[1], bernhard.klein@tu-dresden.de[2], dirk.plettemeier@tu-dresden.de[3]

2. THEORY

2.1 Derivation of permittivity and relation to propagation constant

Considering a transversal-electromagnetic (TEM) wave propagating through an homogeneous and otherwise arbitrary material, we will use the time-harmonic version of the Maxwell-Ampere equation

$$\nabla \times H = J + j\omega D = J_i + J_c + j\omega\varepsilon E \qquad (1)$$

to derive the most general expression for the complex permittivity. E and H represent the electric and magnetic field, respectively, and $D = \varepsilon E$ denotes the electric displacement field with the permittivity ε. $J = J_i + J_c$ stands for the total electric current density consisting of the impressed electric current density J_i and the conduction electric current density $J_c = \sigma_c E$. The field conductivity and the angular frequency are given by σ_c and ω, respectively.

The complex permittivity of an arbitrary material is given by

$$\varepsilon = \varepsilon' - j\varepsilon'' = \varepsilon_0\varepsilon_r = \varepsilon_0(\varepsilon_r' - j\varepsilon_r''), \qquad (2)$$

where ε_0 stands for the vacuum permittivity and ε_r for the relative permittivity of the material. The primed and double primed characters denote the real and imaginary parts of the related quantity.

Combining (1) with (2) and assuming no electrical current sources are present in the material ($J_i = 0$) gives

$$\nabla\times H = j\omega\varepsilon' E + (\sigma_c + \omega\varepsilon'')E = j\omega\varepsilon'(1 - j\frac{\sigma_{eq}}{\omega\varepsilon'})E, \quad (3)$$

where $\sigma_{eq} = \sigma_c + \omega\varepsilon''$ stands for the equivalent conductivity seen by any electromagnetic wave propagating through the material, which consists of a term σ_c covering the "metallic conductivity" and a term $\omega\varepsilon''$ covering the "dielectric conductivity".

The effective loss tangent is then defined as

$$\tan\delta = \frac{\sigma_{eq}}{\omega\varepsilon'} = \frac{\sigma_c}{\omega\varepsilon'} + \frac{\varepsilon''}{\varepsilon'} = \tan\delta_c + \tan\delta_d. \qquad (4)$$

By using this formulation, loss due to (metallic) conductivity[1] related to $\tan\delta_c = \frac{\sigma_c}{\omega\varepsilon'}$ can be distinguished from dielectric loss[2] related to $\tan\delta_d = \frac{\varepsilon''}{\varepsilon'}$.

Considering a non-magnetic material (relative permeability $\mu_r = 1$), the propagation constant is given as

$$\gamma = j\frac{\omega}{c} = j\omega\sqrt{\mu_0\varepsilon} = j\omega\sqrt{\mu_0\varepsilon_0\varepsilon_r'(1 - j\tan\delta)}, \quad (5)$$

where μ_0 stands for the vacuum permeability and c for the velocity of light inside the material. Since the propagation constant is a complex quantity consisting of a loss constant α and a phase constant β, it can also be written as

$$\gamma = \alpha + j\beta, \qquad (6)$$

and by combining (5) with (6) one obtains the useful relations

$$\mathrm{Re}\{\gamma^2\} = \alpha^2 - \beta^2 \qquad (7)$$

$$\mathrm{Im}\{\gamma^2\} = 2\alpha\beta. \qquad (8)$$

These two equations can be combined with (5) and lead to relations for the real and imaginary part of the relative permittivity:

$$\varepsilon_r' = -\frac{\mathrm{Re}\{\gamma^2\}}{\omega^2\mu_0\varepsilon_0} \qquad (9)$$

$$\varepsilon_r'' = -\frac{\mathrm{Im}\{\gamma^2\} - \omega\mu_0\varepsilon_0\sigma_c}{\omega^2\mu_0\varepsilon_0} \qquad (10)$$

2.2 Extraction of propagation constant out of S-Parameter measurements

Using signal flow graph theory, useful relations between S-Parameters and transmission (T) as well as reflection (Γ) coefficient can be found [1]:

$$S_{11} = S_{22} = \frac{(1 - T^2)\Gamma}{1 - \Gamma^2T^2} \qquad (11)$$

$$S_{21} = S_{12} = \frac{(1 - \Gamma^2)T}{1 - \Gamma^2T^2} \qquad (12)$$

Combining (11) and (12), the coefficients can be expressed by the S-Parameters:

$$T = \frac{(S_{11} + S_{21}) - \Gamma}{1 - (S_{11} + S_{21})\Gamma} \qquad (13)$$

$$\Gamma = K \pm \sqrt{K^2 - 1} \qquad (14)$$

$$K = \frac{S_{11}^2 - S_{21}^2 + 1}{2S_{11}}, \qquad (15)$$

where the sign in (14) is chosen so that $|\Gamma| \leq 1$, which is required for causal, passive materials.

Since a single TEM mode of propagation in a TL is being assumed, the transmission coefficient is given by

$$T = e^{-\gamma\, l}, \qquad (16)$$

where l is the length of the TL. The propagation constant can be calculated from (16) in a direct manner

$$\gamma = -\frac{\ln(T)}{l} = -\frac{1}{l}\Big[\ln(|T|) + j[\varphi(T) + 2\pi n]\Big], \quad (17)$$

where $n \in \mathbb{Z}$ and c_0 stands for the velocity of light in vacuum. Due to the ambiguous nature of the complex logarithm, (17) becomes a multivalued problem. The resulting phase ambiguity can easily be solved using phase unwrapping and offset correction of the phase to ensure causality.

[1] e.g. loss due to collision of electrons with other electrons and atoms

[2] e.g. loss due to motion respective heat, which occurs because of dielectric relaxation effects

2.3 Application of this theory to planar transmission line measurements and limitations thereof

Ultimately, γ obtained by measurement as in (17) can be used in combination with (9) to determine ε_r'.

However, the previously developed theory and equations only hold true on condition of a single TEM mode of propagation, i.e. a TEM wave propagating through a material with an homogeneous cross-section. This cannot be satisfied in a straight manner by a planar TL.

Nonetheless, most lines of this kind can be assumed to work in a quasi-TEM mode[3] with effective material parameters modeling a homogeneous cross-section, as long as single mode operation is maintained and higher order modes are sufficiently suppressed[4]. In this case, ε_r in (9) and (10) is replaced by $\varepsilon_\mathrm{r,eff}$ of the TL's equivalent cross-section, and the actual ε_r' of the substrate material can be obtained by comparison with numerical simulations after measurement, as we will show in section 4.

Considering the loss of the dielectric substrate material related to ε_r'', we cannot simply apply the aforementioned procedure for ε_r'. Since the cross-section of a planar TL consists of metallic (e.g. the TL's central conductor) as well as dielectic (e.g. air above and beside the central conductor and substrate below the conductor) areas, the effective cross-section shows a mixture of both loss effects. Literature [7], [8] usually distinguishes between a good conductor ($\frac{\sigma_{eq}}{\omega\varepsilon'} >> 1$) and a good dielectric ($\frac{\sigma_{eq}}{\omega\varepsilon'} << 1$) here, assuming the material is homogeneous within it's cross-section. This approach cannot be applied to the effective cross-section of a planar TL.

To be able to calculate ε'' using the general equation as given in (10), we would have to extend the term σ_c to cover for some kind of effective conductivity of the cross-section $\sigma_\mathrm{c,eff}$, which could be seen as an approach similar to the effective permittivity method. This task is very ambitious and requires a development of a completely new theory as well as extensive modifications of available simulation tools. Since, moreover, one is usually more interested in the overall loss or effective $\tan\delta$ of a transmission line rather than the substrate's $\tan\delta_d$, the authors decided to account for the losses in the planar TLs by calculating the overall loss directly from the measured propagation constant

$$\alpha = \mathrm{Re}(\gamma). \tag{18}$$

Following the presented approach, a measurement of the S-Paramaters of a TL allows for a fast calculation of the effective permittivity of the related substrate as well as the overall TL loss.

[3] Field components in longitudinal direction are existent, but are neglectable in comparison to the transverse components.

[4] We will give useful relations how to avoid multi-modal behaviour in a planar transmission line in section 3.

3. HIGHER ORDER MODES IN TL

Besides the fundamental quasi-TEM mode, several types of higher order modes in planar TLs exist [9–13]:

3.1 Surface waves

Concerning all planar TLs employing a dielectric-conductor interface (e.g. MS, GCPW, CPW[5]), even the fundamental modes will always radiate power into the substrate. Besides that, grounded dielectric slab modes propagating alongside the aforementioned interface can be an issue, as coupling with the desired fundamental mode can occur. Hence, these modes could introduce resonance effects and increase loss due to leakage. They are often referred to as so called surface waves, as the field strength of these modes decays exponentially outside the dielectric slab [10]. Their cutoff frequencies for the TM and TE case are given by [11]

$$f_{c,\mathrm{TM_n}} = \frac{c_0 n}{2h\sqrt{\varepsilon_r - 1}} \tag{19}$$

$$f_{c,\mathrm{TE_n}} = \frac{c_0(1+2n)}{4h\sqrt{\varepsilon_r - 1}}, \tag{20}$$

where $n \in \mathrm{N}_0$ and h denotes the height of the dielectric slab, which is the substrate height for a related TL. As can be seen from these equations, the TM_0 mode has zero cutoff frequency and hence is propagable simultaneously with the fundamental quasi-TEM mode of the TL. Coupling from the fundamental mode to this first surface wave and thus leakage due to radiation occurs after a frequency of [11]

$$f_{r,\mathrm{TM_0}} = \frac{c_0 \arctan(\varepsilon_r)}{\pi h\sqrt{2(\varepsilon_r - 1)}}, \tag{21}$$

which gives a useful relation for TL design.

Besides that, discontinuities along the line can always introduce coupling with the TM_0 mode and thus unwanted radiation or loss. In addition, standing surface waves can be reflected at the substrate's boundaries or conductive structures along the modes' propagation path, which could introduce standing surface waves. This might introduce a slight ripple in the attenuation characteristics and is especially true for MS or similar parallel plate modes [11] (see next item).

3.2 Substrate modes

For TLs with two conductive boundaries (such as MS or GCPW), higher order substrate modes form another group of undesired modes. They propagate

[5] For the following explanations, non-ideal CPW and GCPW with finite top ground width are assumed.

in-between the structure given by the top and ground metallization, which can be seen as a parallel plate TL, hence they are often referred to as parallel plate (PPL) modes [12].

For MS, these modes are - besides the other, parasitic modes - the true higher order modes of the fundamental MS mode (see Fig. 1, a-c). They exist in lateral direction beneath the MS conductor and their cutoff frequencies are given by [11]

$$f_{c,\mathrm{MS}} = \frac{c_0 n}{2w_{\mathrm{eff}}\sqrt{\varepsilon_{r,\mathrm{eff}}}}, \tag{22}$$

where w_{eff} stands for the effective strip width of the MS conductor [6]. Due to fringe fields in the air and near the corners of the top metallization, not all of the field is confined in the substrate. The effective width and permittivity corrects for this effect in comparison to an ideally confined PPL mode and therefore has to be taken into account here.

For GCPW, two different substrate modes exist [12]: A PPL mode very similar to the MS modes (see Fig. 1, c) and a mode in the substrate height direction (see Fig. 1, d). The PPL modes are given due to a difference in top and ground potential, which is basically the same condition as for MS. Again, these modes exist in lateral direction beneath the top conducting plane and have cutoff frequencies [13], [14]

$$f_{c,\mathrm{GCPW,PPL}} = \frac{2c_0 m}{w_{\mathrm{tot}}\sqrt{2(\varepsilon_r - 1)}}, \tag{23}$$

where $m \in \mathrm{N}_{>0}$ and w_{tot} denotes the total width of the GCPW top metallization including strip, gap and ground width. This kind of higher order (PPL) mode can be understood in the same way as for MS, if the top conductor area given by w_{tot} is interpreted as effective width w_{eff} of an equivalent MS strip (see Fig. 1, c).

The substrate modes in direction of the substrate height have cutoff frequencies [13], [14]

$$f_{c,\mathrm{GCPW,h}} = \frac{c_0 m}{h\sqrt{2(\varepsilon_r - 1)}}. \tag{24}$$

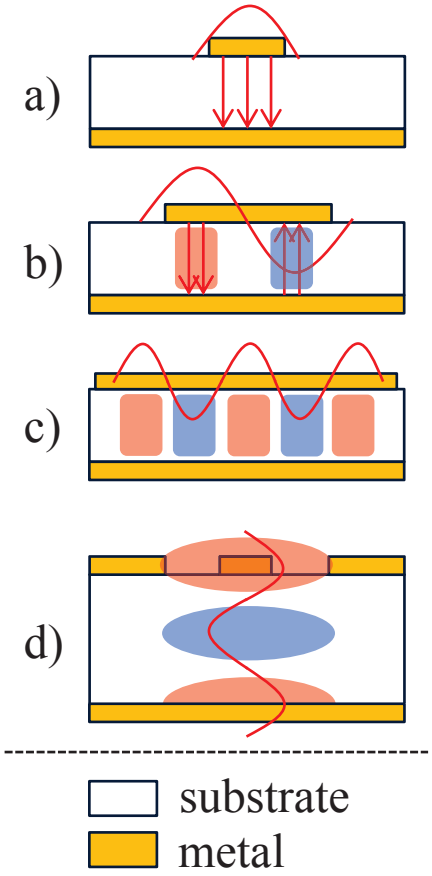

Fig. 1: *Schematic illustration of modes in cross-sectional view of MS, GCPW: Red arrows indicate electric field vectors (neglecting fringe fields), red lines indicate the wavelength of a wave propagating through the structure, red and blue bars/circles indicate modal field distribution. a) shows the fundamental MS mode. b) shows the first higher order mode in MS (PPL mode) due to widening of the central strip or increasing the frequency. c) shows an arbitrary higher order MS mode using this illustration scheme. d) extends this illustration scheme to an arbitrary higher order GCPW mode.*

4. MEASUREMENT AND SIMULATIONS

4.1 Setup and measurement method

The TLs used during our measurements have been designed following the rules given in section 3 to assure quasi-TEM behavior, see Tab. 1 for relevant sizes.

The measurements were carried out using GGB Picoprobes® Model 67A with a pitch of 400μm and a Network Analyzer up to 67 GHz on a wafer prober station, see Fig. 2 for an exemplary measurement on GCPW.

The TLs with relevant sizes given in Tab. 1 have been fabricated on a commercially available RF substrate (Rogers Corp. RO4003C™,[15]). For MS and GCPW, custom contact pads including vias connecting the top and bottom ground ensured a proper transfer of the probe's ground tips potential to the actual bottom ground. In addition, the GCPW has been fabricated with a via fence extending on both sides for the whole length of the GCPW. The vias have been placed in 600μm distance from the middle of the central conductor. The layouts of the TLs can be seen schematically in Fig. 3.

For calibration, the multiline TRL technique [16] has been implemented and used. By relying on TRL as calibration technique and choosing the thru standard to zero length, the reference plane of the actual measurement can be shifted from the probe tips onto the TL. This allows us to use the theory presented

Table 1: *Measured TLs on RO4003C™.*

	MS	GCPW	CPW
substrate height	203 µm	203 µm	508 µm
width	372 µm	280 µm	180 µm
gap	none	160 µm	130 µm
top gnd width	none	300 µm	300 µm

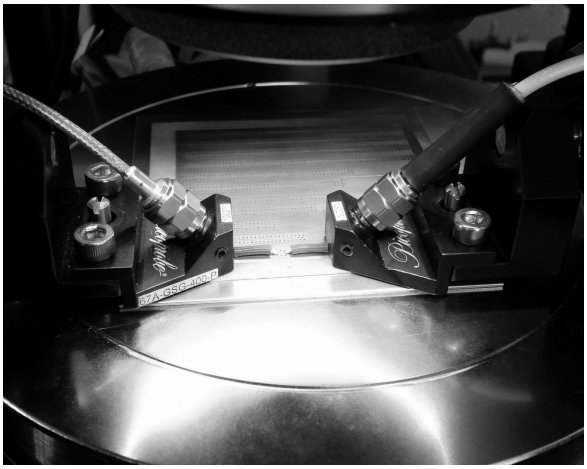

Fig.2: *Measurement of GCPW using HF probes on a wafer prober.*

in section 2, as it effectively cancels out the disturbance introduced by the probe-TL interface during measurement.

To ensure a reliable calibration and be able to perform measurements over the whole frequency range up to 67 GHz, a custom set of calibration standards has been fabricated on the same substrate for each TL. The calibration set consisted of a virtually zero length thru, a shorting bar reflect and three line standards to cover the frequency range from 0.55 GHz to 67 GHz and to comply with the unambiguity condition of line standards [17]. The zero length thru has

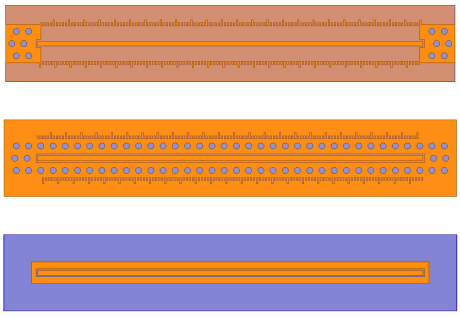

Fig.3: *Layouts of measured TLs: MS, GCPW and CPW (top to bottom). The etched scales in the MS and GCPW layout were necessary for further investigations and are not relevant for the results presented in this paper.*

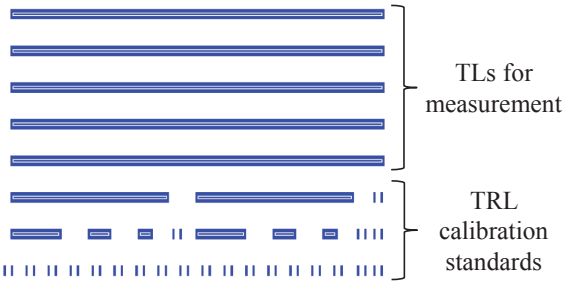

Fig.4: *Exemplary CPW layout consisting of several TLs for measurement as well as a set of related custom calibration standards.*

been chosen to have a length of 1mm, so that the reference plane is shifted onto the TL and strong probe-probe crosstalk can be safely neglected (based on our lab experience), see Tab. 2 for relevant sizes of related calibration standards and Fig. 4 for an exemplary overall layout.

Due to fabrication issues concerning the probe-MS interface structure on the substrate, MS lines in close proximity showed coupling and thus resonance effects in the measurement data. Since this applied to the MS calibration lines as well, we were only able to get reliable MS measurement data up to 24 GHz. GCPW and CPW have been measured up to 67 GHz.

Table 2: *TRL calibration standards on RO4003C™.*

standard	physical length	operating range
thru	1 mm	∞
reflect	0.3 mm	∞
line 1	20.89 mm	0.56 - 4.44 GHz
line 2	5.97 mm	2.22 - 17.77 GHz
line 3	2.16 mm	9.55 - 76.44 GHz

Each TL type was fabricated in physical lengths[6] $l = \{25, 50\}$ mm several times, which allowed us to do multiple measurements on the same structure. As a consequence, deviations in the measurement data due to measurement errors (e.g. placement of probe tips) and effects introduced by inhomogeneous fabrication of a single TL type over the whole substrate (such as slightly different etching) can be minimized by averaging. For that reason, the results displayed in this paper are averaged over those measurements of the same TL type.

The MS and GCPW have been fabricated on the same substrate, whereas the CPW has been fabricated on a substrate of the same material, but different height (see Tab. 1) to ensure a proper substrate height and hence CPW behavior. The MS

[6] This relates to effective lengths of $l = \{24, 49\}$ mm after calibration and shifting the reference plane using the zero length thru.

and GCPW have been measured directly on the wafer prober with the integrated vacuum turned on, whereas the CPW was placed on a Rohacell® block ($\varepsilon_r \approx 1$) of about 1cm height on the wafer prober during measurement to keep a distance to the metallic surface of the wafer chuck to prevent GCPW behaviour.

4.2 Effective permittivity and mapping procedure

For the sake of a clear understanding of this section, we first want to give a brief summary of the overall procedure: First, the S-Parameters of the TL under investigation are measured. Then, signal flow theory is applied to extract the transmission and reflection coefficient, which allow for a calculation of the propagation constant. The propagation constant then allows for a determination of the effective permittivity and loss. In a subsequent mapping procedure, the beforehand implicitly measured effective permittivity is mapped to the physical value of the substrate material extracted from simulation data and compared to the value given by approximate models known from publications.

Results for $\varepsilon_{\mathrm{r,eff}}$ of the TL can be seen in Fig. 5. The values for the $\varepsilon_{\mathrm{r,eff}}$ of MS and CPW at lower frequencies agree very well with quasi-static approximations as given in [6].

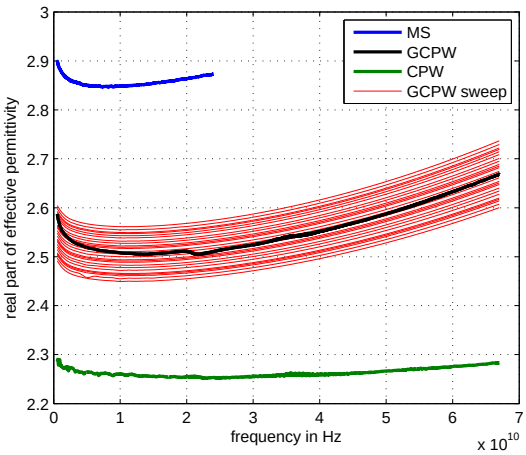

Fig. 5: *Calculated $\varepsilon_{r,eff}$ from measurement data of TLs. Slight ripple in the graphs (e.g. for GCPW near 20 GHz) is expected to be due to calibration inaccuracies.*

To map the implicitly measured $\varepsilon_{\mathrm{r,eff}}$ to the desired physical value of ε_{r}, the TLs have been modeled and simulated using the commercially available full-wave simulator Ansys® HFSS. The modeled substrate permittivity has been swept in a reasonable range with a step size of 0.01. The S-Paramaters obtained during simulation allowed for a calculation of $\varepsilon_{\mathrm{r,eff}}$ as presented before. The $\varepsilon_{\mathrm{r,eff}}$ obtained during measurement is then compared to the ones calculated from simulation data (see exemplarily for GCPW the red lines in Fig. 5) and mapped to the closest result.

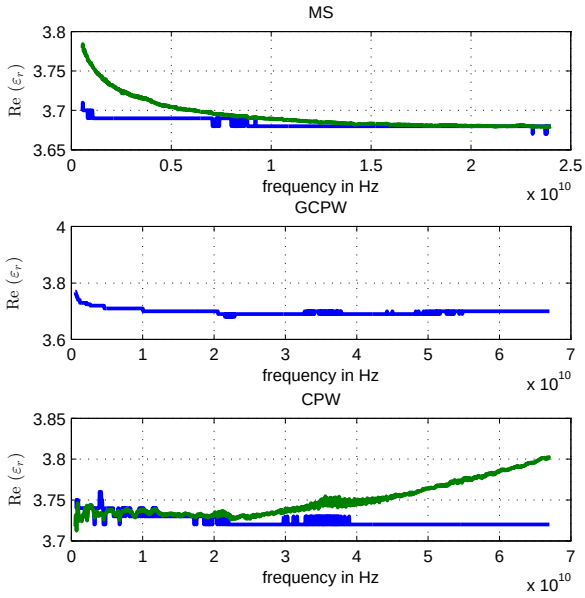

Fig. 6: *Mapped $\varepsilon_{r,eff}$ using our method (blue) and TL-related dispersion models (green).*

4.3 Comparison with dispersion models

For comparison, results given by known dispersion models for MS [3] and CPW [5] are shown in Fig. 6 as well. The data given for our method (blue lined) clearly looks not physically correct, as the peaks are due to the parameter sweep with 0.01 step size and not of physical origin. This effect can be compensated by a smaller step size or a slight curve fitting to smoothen the curve, both of which seemed not reasonable to the authors, as 0.01 gives a precise enough value and is being assumed to lie near the accuracy bounds of the actual measurement. For future investigations, the authors plan to interpolate the simulation results to obtain a smooth and physically correct curve. For GCPW including vias, no reliable dispersion model could be found by the authors. GCPW models given by publications such as [4] only apply for GCPW without vias.

The MS model shows good agreement with our results only for the higher end of the measured frequency span and seems to overestimate the ε_r for lower frequencies, we assume this is due to it's approximative nature. The original publication [3] only evaluated the model on a certain set of geometry parameters and up to 60 GHz. As could be seen during our simulations, this model seems to converge to the ε_r determined by our method with good accuracy. Therefore, the result obtained by it for the higher end of the measured frequency span has been used

as an initial guess for the parameter sweeping range during the GCPW and CPW simulations.

The CPW model shows good agreement for lower frequencies, but significant deviation for higher ones, which we assume is due to the quasi-static assumptions of the model. Nevertheless, it lies within the proximity of the results obtained by our procedure. Since we used a substrate of the same material but different height for fabrication of the CPW, there is a slight difference between ε_r for the substrate with MS and GCPW and the substrate with CPW. This can be explained by RO4003C$^{\text{TM}}$fabrication tolerances [15].

4.4 Loss

The loss calculated using (18) for the three TL types can be seen in Fig. 7. The MS and GCPW loss agree very well for the frequencies measured, whereas MS shows a little less loss than GCPW. Radiation as well as dielectric loss should be neglectable in the frequency range the MS has been measured, hence the conductor loss is assumend to contribute mostly to the calculated overall loss. Since the conductive boundaries for MS and GCPW are similar in their dimensions, the assumption of similiar loss for both TL seems reasonable.

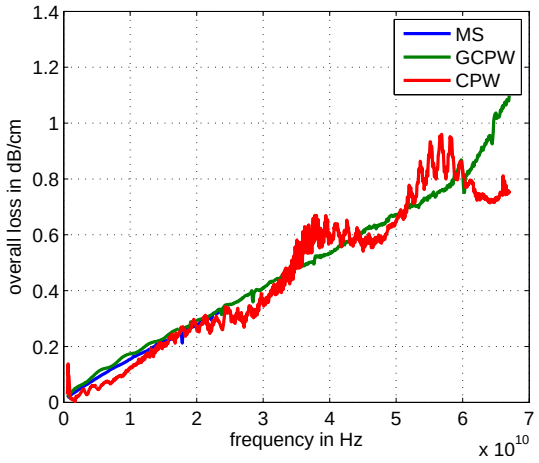

Fig. 7: *Overall loss calculated from S-Parameter measurements of the TL.*

The CPW loss shows peaks reoccuring for distinct frequencies, which suggests some kind of resonance effect, e.g. coupling to higher order modes as explained in section 3.

For a first explanation, one could assume surface waves causing the ripple. In direct comparison to the MS attenuation curve, which should exhibit this effect as well, no ripple can be seen. If this first explanation should hold true, this additional observation could only be explained by the different substrate heights for MS and CPW, which seems rather speculative.

The second explanation arises from a comparison with the GCPW: A similar ripple - though significant smaller - can be seen in the attenuation curve at about the same frequencies[7] (e.g. near about 7GHz), which suggests some (G)CPW related effect to cause the ripple. This effect is clarified by a coupled slotline mode, which can exist if there is a potential difference between the two top ground conductors of a (G)CPW introduced by asymmetric probe tip placement, discontinuities or unequal top ground widths along the TL [6], [18]. This mode can propagate the same as the fundamental quasi-TEM CPW mode up from DC and is usually suppressed by the use of air bridges or vias. For the CPW, the potential difference and thus undesired mode can easily be introduced by the aforementioned reasons - especially asymmetric probe tip placement - and thus coupling to the fundamental mode can occur, which appears as ripple in the attenuation curve. For GCPW, the vias should in theory suppress this mode completely - nevertheless, slight potential differences might occur due to asymmetric probe tip placement as well or inaccurate via placement. Therefore, only a slight influence and ripple in the attenuation curve occurs. The authors take this argumentation as reasonable explanation for the observed ripple.

5. CONCLUSION

A general workflow for extracting the relative permittivity as well as the loss of planar TLs out of S-Parameter measurements has been shown. Since this theory can only be used for quasi-TEM wave propagation, design rules to suppress undesired higher order modes in planar TL have been given.
Different TLs have been measured up to 67GHz and the related substrate permittivity ε_{r} as well as overall loss could be determined using the presented method. Deviations in the loss have been related to undesired modes propagating along the TL, with CPW and GCPW showing slight ripple in the attenuation curve. Concerning the permittivity, the results for MS and GCPW on RO4003C$^{\text{TM}}$agree very well. The data for CPW on a substrate of the same material, but different height, shows comparable results as well and differences are assumed to arise only from fabrication tolerances. Our results represent the physical conditions of the measured TLs properly, since full-wave analysis of the actual structures has been used for the dispersion mapping.

Since we use the same method to map S-Parameters to $\varepsilon_{\text{r,eff}}$ for measurement as well as simulation data, errors due to our method are neglectable and may only be introduced by measurement and possible simulation inaccuracies.

Although models known from publications lie within the near proximity of our results, they show clear deviations for very low and higher frequencies. This is expected to worsen with increasing frequency,

[7] Deviations in frequency here may occur due to slightly different substrate permittivity and height.

as the accuracy of the fitted models decreases. Thus, the presented approach gives an accurate, broadband and fast implemented alternative to provide a dispersion mapping, which should be scalable to higher frequencies. We will investigate this further in future publications.

ACKNOWLEDGEMENT

This work is partly supported by the German Research Foundation (DFG) within the Cluster of Excellence 'Center for Advancing Electronics Dresden'.

References

[1] A. Nicolson and G. F. Ross, "Measurement of the intrinsic properties of materials by time-domain techniques," in *IEEE Trans. Instrum. Meas.*, vol. 19, no. 4, pp. 377-382, Nov. 1970.

[2] A.-H. Boughriet, C. Legrand, and A. Chapoton, "Noniterative stable transmission/reflection method for low-loss material complex permittivity determination," in *IEEE Trans. Microw. Theory Tech.*, vol. 45, no. 1, pp. 52-57, Jan. 1997.

[3] M. Kirschning and R. Jansen, "Accurate model for effective dielectric constant of microstrip with validity up to millimetre-wave frequencies," in *Electron. Lett.*, vol. 18, no. 6, pp. 272-273, Mar. 1982.

[4] M. Frankel, S. Gupta, J. Valdmanis, and G. Mourou, "Terahertz attenuation and dispersion characteristics of coplanar transmission lines," in *IEEE Trans. Microw. Theory Tech.*, vol. 39, no. 6, pp. 910-916, Jun. 1991.

[5] W. Heinrich, "Quasi-TEM description of MMIC coplanar lines including conductor-loss effects," in *IEEE Trans. Microw. Theory Tech.*, vol. 41, no. 1, pp. 45-52, Jan. 1993.

[6] K. C. Gupta, "Microstrip lines I: Quasi-Static analyses, dispersion models, and measurements," in *Microstrip Lines and Slotlines 2nd Ed.*, Artech House Microwave Library, 1996.

[7] C. A. Balanis, "Electrical Properties of Matter," in *Advanced Engineering Electromagnetics*, John Wiley & Sons, 2002.

[8] J. D. Jackson, "Plane Electromagnetic Waves and Wave Propagation," in *Classical Electrodynamics*, John Wiley & Sons, 1998.

[9] M. Riaziat, R. Majidi-Ahy, and I.-J. Feng, "Propagation modes and dispersion characteristics of coplanar waveguides," in *IEEE Trans. Microw. Theory Tech.*, vol. 38, no. 3, pp. 245-251, Mar 1990.

[10] E. Godshalk, "Surface wave phenomenon in wafer probing environments," in *ARFTG Conf. Digest-Fall, 40th*, vol. 22, Dec 1992, pp. 10-19.

[11] R. K. Hoffmann, "Higher Order Modes on Microstrip," in *Handbook of Microwave Integrated Circuits*, Artech House Microwave Library, 1987.

[12] W. Heinrich, F. Schnieder, and T. Tischler, "Dispersion and radiation characteristics of conductor-backed CPW with finite ground width," in *Microwave Symp. Digest. 2000 IEEE MTT-S Int.*, vol. 3, Jun. 2000, pp. 1663-1666.

[13] F. Schnieder, T. Tischler, and W. Heinrich, "Modeling dispersion and radiation characteristics of conductor-backed CPW with finite ground width," in *IEEE Trans. Microw. Theory Tech.*, vol. 51, no. 1, pp. 137-143, Jan. 2003.

[14] T. Tischler, "Die perfectly-matched-layer-randbedingung in der Finite-Differenzen-Methode im Frequenzbereich: Implementierung und Einsatzbereiche," Ph.D. dissertation, Technische Universität Berlin, Berlin, Germany, 2004.

[15] *Rogers Corporation - Data sheet: RO4000® Series - High Frequency Circuit Materials.*

[16] R. B. Marks, "A multiline method of network analyzer calibration," in *IEEE Trans. Microw. Theory Tech.*, vol. 39, no. 7, pp. 1205-1215, Jul. 1991.

[17] *Agilent Product Note 8720-2: In-fixture Microstrip Device Measurement Using TRL Calibration.*

[18] G. Ponchak, J. Papapolymerou, and M. Tentzeris, "Excitation of coupled slotline mode in finite-ground CPW with unequal ground-plane widths," in *IEEE Trans. Microw. Theory Tech.*, vol. 53, no. 2, pp. 713-717, Feb. 2005.

Patrick Seiler received a B.Sc. and M.Sc. degree in Electrical Engineering from Technical University Berlin, Germany, in 2011 and 2012, respectively. During his master's degree studies, he was with the Chair of High Frequency Engineering and Photonics and worked on photonic integrated circuits, e.g. coherent photonic receivers in Silicon-on-Insulator nano waveguide technology. Since 2013, he is a research associate at the Chair for RF Engineering of Technical University Dresden (TUD), Germany. He is currently working towards his PhD within a project inside TUD's newly founded Cluster of Excellence "Center for Advancing Electronics Dresden (cfaed)". His current research interests include (hybrid) material characterization as well as on-wafer measurement techniques in the high frequency domain.

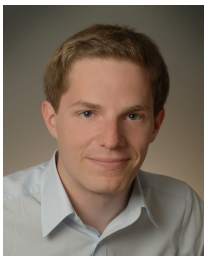

Bernhard Klein was born in Germany in 1988. He received his Diploma degree in Electrical Engineering at the University of Technology Dresden (TUD), Germany in 2013. In 2012 he was with the IBM Zurich Research Laboratory, Rüschlikon, Switzerland where he implemented various integrated antenna designs for a THz-imaging system. In 2011, he investigated radar-backscattering in the human body depending on body movements at the Chair for RF Engineering at the Communications Laboratory of TUD in cooperation with SIEMENS Healthcare, Germany. In 2013, he joined the Chair for RF Engineering at the University of Technology Dresden (TUD), Germany, where he is working on integrated antenna designs in the mm- and submm-wavelength regime. He is an alumnus of the German National Academic Foundation.

Dirk Plettemeier received a diploma in Communication Engineering from the University of Applied Sciences in Lemgo and a diploma in Electrical Engineering from the University of Bochum. He received his Ph.D. degree from the University of Bochum in 2002. Dirk Plettemeier was employed at the Institute for High-Frequency Technique / Department of Antennas and Wave Propagation at University of Bochum until 2003. From 2003 until 2007 he was head of the research group Numerical Calculation of High Frequency Electromagnetic Fields and Waves at the Electrotechnical Institute / Chair and Laboratory for Theory of Electromagnetic Fields and EMC at TU Dresden (TUD). From 2007 to 2011 he was head of the department High Frequency Engineering - Antennas and Wave Propagation at the Communication Laboratory / Chair of RF and Photonics at TUD. Since 2011 he is head of the Chair of RF Engineering at TUD.